X-ray luminescence of SrF$_2$:Eu nanopowders

© A.R. Drobysheva[1], Yu.A. Ermakova[1], A.A. Alexandrov[1], V.V. Voronov[1], S.Ch. Batygov[1], A.D. Rezaeva[1],
A.K. Martyanov[1], V.S. Sedov[1], I.A. Tiazhelov[1], K.N. Boldyrev[2], N.Yu. Tabachkova[1], S.V. Kuznetsov[1,¶]

[1] Prokhorov General Physics Institute of the Russian Academy of Sciences, Moscow, Russia
[2] Institute of Spectroscopy of the Russian Academy of Sciences,
108840 Troitsk, Moscow, Russia
¶ e-mail: kouznetzovsv@gmail.com

Concentration series of single-phase SrF$_2$:Eu solid solutions with a particle size of ≈ 50 nm were synthesized by precipitation from aqueous solutions. The bands of europium in the di- and trivalent states as well as a band of intrinsic exciton luminescence of strontium fluoride were identified in the X-ray luminescence spectra. The most intense luminescence band is the band of trivalent europium with a maximum at $585-590$ nm which corresponding to the $^5D_0 \rightarrow {}^7F_1$ transition. The highest X-ray luminescence intensities upon excitation by an X-ray tube with silver and tungsten anodes are achieved for compositions containing about 15.0 mol.% and 7.5 mol.% europium, respectively.

Keywords: X-ray luminescence, strontium fluoride, europium.

Introduction

In the last decade, there has been a sharp jump in the use of X-ray free-electron lasers to study biomolecules and the crystal structure of various materials. Progress has been made by increasing the number of such lasers and increasing their power [1–6]. In general, an increase in the output power of X-ray lasers and synchrotrons dictates the need to develop efficient and stable X-ray luminescent screens for visualizing intense beams and their precise focusing on the object under study [7]. For these purposes, bulk crystalline materials are currently used, which degrade rather quickly under the influence of high-power X-rays. This is mainly due to their low thermal conductivity, which leads to the impossibility of dissipation of the released heat and sharp local heating on the surface or in the bulk of the crystal [8].

Radiation-resistant materials for X-ray luminescent screens should have intense X-ray luminescence, high thermal conductivity, chemically stable when heated and under the influence of ionizing radiation [9]. The most suitable for this application are diamond matrix composites with interstitial nanoparticles [10–12]. The diamond matrix ensures record thermal conductivity, chemical stability over a wide temperature range, and low intrinsic absorption in the X-ray range [13–18]. The interstitial particles demonstrate intense X-ray luminescence in the visible range of the spectrum due to the use of both doping rare-earth components in their composition and upon excitation of the matrix itself.

Use of pure phosphors such as EuF$_3$ [12], HoF$_3$ [19], CeF$_3$ [19], europium oxide obtained by decomposition of europium 2,6-pyridinedicarbonate [20] or Eu(DPA)$_3$ [21]

leads to the production of luminescent composites, but their intensity is limited by the effects of concentration quenching. A more efficient method for obtaining luminescent composites is the introduction of particles with an optically inactive matrix doped with active rare-earth ions with a concentration that demonstrates the highest luminescence intensity. For implementation, it is required to use substances that withstand high temperatures of CVD diamond growth in microwave plasma $(700-1000\,°C)$ [22] without their degradation as a result of melting, evaporation, decomposition, and phase transformations [9]. Fluorides doped with rare-earth elements are the most promising for studying as part of solving the proposed problem, since they have a lower crystal lattice phonon energy than oxides. The use of substances with a lower phonon energy than fluorides, such as chlorides, bromides and iodides, is limited by the fact that most of them decompose at temperatures above $700\,°C$, and are also unstable in air. For the fluorides studied earlier [12,23] (EuF$_3$ and NaGdF$_4$:Eu), low-temperature modifications were used, which, under the conditions of diamond growth, could experience a phase transition to high-temperature modifications. To exclude from consideration of the nature of luminescent processes the effects of phase transformations of embedded particles under the conditions of diamond growth, difluorides were chosen as matrices, which have a high isomorphic capacity with respect to rare-earth elements [24] and do not possess phase transformations. Strontium fluoride has a higher melting point $1464\,°C$ [25] compared to calcium fluoride $1418\,°C$ [26], barium fluoride $1360\,°C$ [27], magnesium fluoride $1263\,°C$ [28] and lead fluoride $822\,°C$ [29]. A solid solution based on strontium fluoride will allow to work with one of the most temperature-resistant fluorides, and the use of europium will
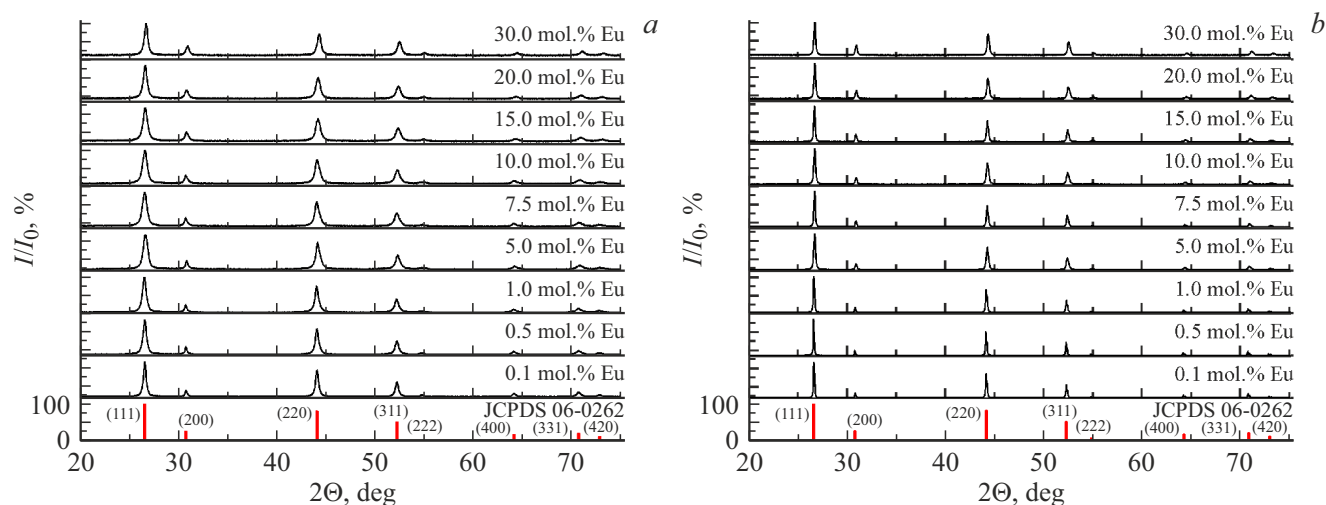
Figure 1. X-ray diffraction patterns of synthesized samples of solid solutions SrF$_2$:Eu and X-ray card JCPDS# 06-0262: *a* — after drying at 45°C, *b* — after heat treatment at 600°C.
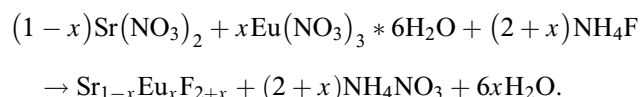
allow a reliable comparison of the spectral and luminescent characteristics of europium with previously studied matrices.

The literature describes procedures for the synthesis of SrF$_2$:Eu solid solutions with different particle sizes. In the paper [30], particles with a size of approximately 7 nm were synthesized by the hydrothermal method. The luminescence spectra show bands corresponding to Eu^{2+} and Eu^{3+}. It was found that at low Eu concentrations broadband Eu^{2+} luminescence dominated with a maximum at a wavelength of 416 nm, while the luminescence intensity of narrow Eu^{3+} bands grew with increasing Eu concentration. Transparent dispersions of hydrophobic nanoparticles SrF$_2$:Eu^{3+} (1−20 mol.%) in cyclohexane with a particle size from 6 to 11 nm [31] and a shell of sodium dodecylbenzenesulfonate were synthesized by the fluorolytic sol-gel method. Bright red luminescence of europium was recorded both upon excitation through sodium dodecylbenzenesulfonate at a wavelength of 278 nm, and in the excitation bands of europium at a wavelength of 393 nm. The total integrated luminescence intensity increased linearly up to Eu^{3+} content 10 mol.%, at a higher concentration (20 mol.% Eu^{3+}) the luminescence intensity continued to increase, but in a non-linear manner. Powders of CaF$_2$, SrF$_2$, BaF$_2$ and PbF$_2$ doped with Eu^{3+} [32] were synthesized mechanochemically in a ball mill without the use of solvents, and the crystallite sizes were estimated to be 10−20 nm (CaF$_2$, SrF$_2$ and BaF$_2$), and for PbF$_2$ − 57 nm. The simplest and most easily scalable production method is the method of precipitation from aqueous solutions, which allows to synthesize bright phosphors based on strontium fluoride doped with rare-earth elements [33–35]. No publications on the synthesis and study of the X-ray luminescence characteristics of powders of SrF$_2$:Eu solid solutions obtained by precipitation from aqueous solutions upon excitation by various X-ray tubes have been found.

The purpose of this paper was to synthesize and study the properties of nanopowders of SrF$_2$:Eu solid solutions by coprecipitation from aqueous solutions in order to determine the compositions that demonstrate the highest X-ray luminescence intensity and are optimal for the manufacture of diamond luminescent composites.

Experimental part

Sr(NO$_3$)$_2$ (99.99%, „Lanhit"), Eu(NO$_3$)$_3$ · 6H$_2$O (99.99%, „Lanhit"), NH$_4$F (chemical pure, „Lanhit") and double-distilled water of our own production. The reagents were used without additional purification steps. A series of nanopowders of SrF$_2$:Eu solid solutions with europium content of 0.1, 0.5, 1.0, 5.0, 7.5, 10.0, 15.0, 20.0, and 30.0 mol.% was synthesized by precipitation from aqueous solutions. Powders of solid solutions SrF$_2$:Eu were obtained by precipitation from aqueous solutions according to the reaction

$$(1-x)\text{Sr}(\text{NO}_3)_2 + x\text{Eu}(\text{NO}_3)_3 * 6\text{H}_2\text{O} + (2+x)\text{NH}_4\text{F}$$

$$\rightarrow \text{Sr}_{1-x}\text{Eu}_x\text{F}_{2+x} + (2+x)\text{NH}_4\text{NO}_3 + 6x\text{H}_2\text{O}.$$

A solution of nitrates (C= 0.08 M) was added dropwise to an ammonium fluoride solution (0.16 M, an excess of 7% of the stoichiometry), which was intensively stirred on a magnetic stirrer 5−10 min. The resulting suspension was stirred on a magnetic stirrer for 2 h. After settling the precipitate, the mother solution was decanted, the precipitate was washed with a 0.5% ammonium fluoride solution with the control of the purity of the washing from nitrate ions by a qualitative reaction with diphenylamine. The washed precipitate was first dried in air at a temperature of 45 °C, and then in platinum crucibles at a temperature of 600 °C for 1 h at a heating rate of 10 °C/min.

Results of Calculation of Lattice Parameters and CSR of SrF_2: Eu Solid Solutions

№ of the sample	Composition	Drying at 45°C		Heat treatment at 600°C	
		a, Å	CSR, nm	a, Å	CSR, nm
1	$Sr_{0.999}Eu_{0.001}F_{2.001}$	5.804(1)	22	5.801(1)	109
2	$Sr_{0.995}Eu_{0.005}F_{2.005}$	5.803(1)	18	5.800(1)	134
3	$Sr_{0.990}Eu_{0.010}F_{2.010}$	5.800(1)	15	5.799(1)	68
4	$Sr_{0.950}Eu_{0.050}F_{2.050}$	5.798(1)	13	5.795(1)	39
5	$Sr_{0.925}Eu_{0.075}F_{2.075}$	5.800(1)	14	5.793(1)	77
6	$Sr_{0.900}Eu_{0.100}F_{2.100}$	5.794(1)	12	5.790(1)	43
7	$Sr_{0.850}Eu_{0.150}F_{2.150}$	5.790(1)	14	5.785(1)	67
8	$Sr_{0.800}Eu_{0.200}F_{2.200}$	5.785(1)	16	5.779(1)	48
9	$Sr_{0.700}Eu_{0.300}F_{2.300}$	5.778(1)	17	5.773(1)	47

X-ray diffraction (XRD) analysis was performed on a Bruker D8 Advance diffractometer with CuKα-radiation. The lattice parameters (a) and the coherent scattering region (CSR) were calculated using the TOPAS software ($R_{wp} < 10$). Transmission electron microscopy (TEM) was performed on a JEM-2100 (JEOL) microscope. The average particle size was evaluated from microphotographs using the ImageJ software for 50 particles. X-ray luminescence spectra of single-phase powders were recorded at room temperature on an FSD-10 minispectrometer („Optofiber") in the range $200-1000$ nm with a resolution of 1 nm under excitation by an X-ray tube with a tungsten anode operating at a voltage of 30 kV and 30 mA, and on a fiber-optic spectrometer Ocean Optics in the range $350-1100$ nm with a resolution of 0.7 nm when excited by an X-ray tube with a silver anode operating at a voltage of 40 kV and a current of 35 mA.

Results

X-ray diffraction patterns of SrF_2: Eu solid solutions with europium content of 0.1, 0.5, 1.0, 5.0, 7.5, 10.0, 15.0, 20.0, and 30.0 mol.%, dried at 45 °C and heat-treated at 600 °C, are presented in Fig. 1. The heat treatment temperature was selected based on the data [33,34,36].

Comparison of the X-ray diffraction patterns of the synthesized samples with the X-ray card of the JCPDS 06-0262 database for SrF_2 revealed their complete agreement, there are no additional reflections, which indicates the synthesis of single-phase samples. The X-ray reflections in Fig. 1, a are strongly broadened, which may indicate the synthesis of nanoscale substances due to the smallness of the coherent scattering regions. The position of X-ray reflections is slightly shifted due to a change in the lattice constants in proportion to the amount of the dope additive. X-ray diffraction patterns of samples heat-treated at 600 °C
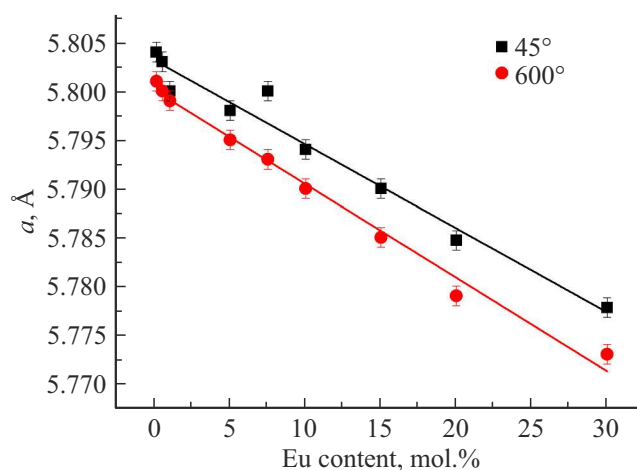

Figure 2. Dependence of the lattice parameters of the SrF_2: Eu solid solution on the Eu content.

are shown in Fig. 1, b. The X-ray reflections are narrower, which indicates an increase in the coherent scattering region and, accordingly, an increase in the particle size. The results of calculating the lattice constants and coherent scattering regions (CSR) are presented in the table.

When comparing the calculation results with the lattice constant of pure strontium fluoride, their regular decrease was revealed due to the fact that the ionic radius of europium is smaller than the ionic radius of strontium [37]. The change in the lattice constants with a change in the europium content is presented graphically in Fig. 2. The coherent scattering regions naturally increase several times during high-temperature treatment. The lattice constants regularly decrease with an increase in the europium content, and heat treatment at 600 °C leads to a decrease in the lattice parameter compared to samples dried at 45 °C. This indicates the volatilization of the ammonium ion, which
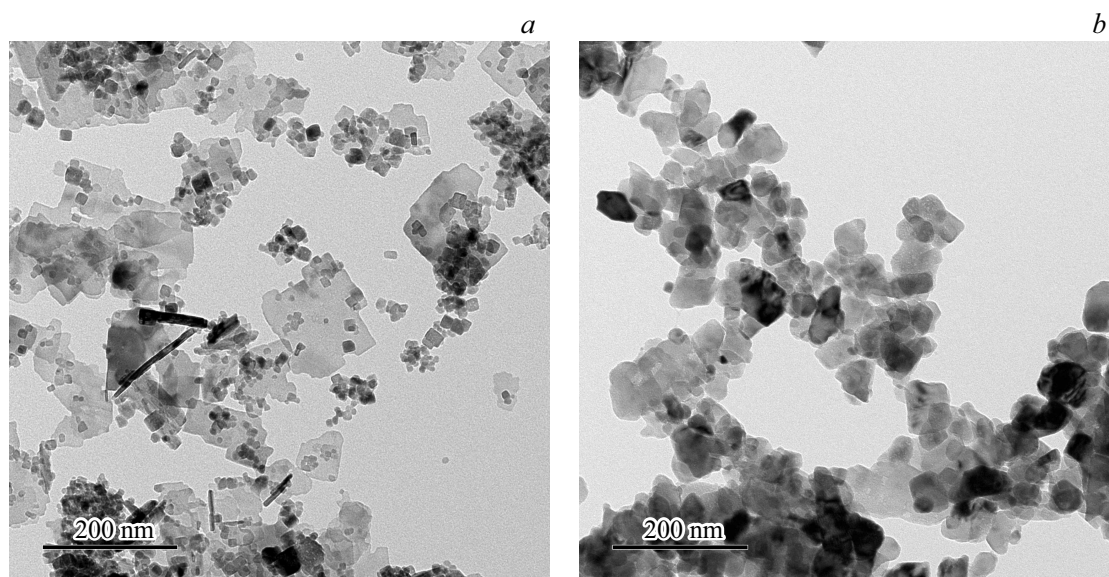
a

b

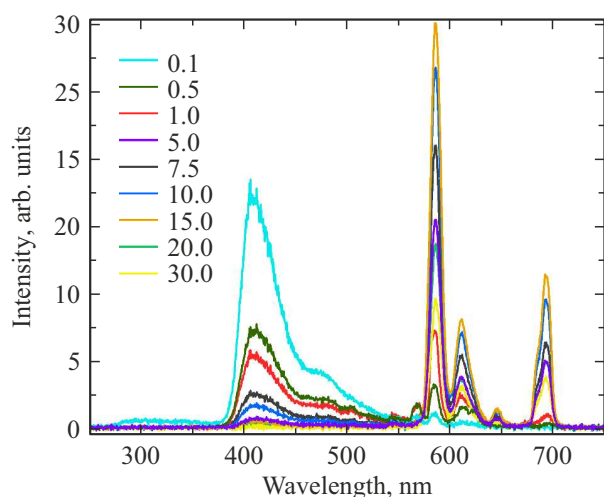**Figure 3.** TEM image of sample $Sr_{0.9}Eu_{0.1}F_{2.1}$: *a* — after drying at $45°C$, *b* — after heat treatment at $600°C$.

Figure 4. X-ray luminescence spectra of the $SrF_2:Eu$ solid solution upon excitation by an X-ray tube with a silver anode. The content of europium in mole percent is presented in the figure.

Figure 5. X-ray luminescence spectra of the $SrF_2:Eu$ solid solution upon excitation by an X-ray tube with a tungsten anode. The content of europium in mole percent is presented in the figure.

can enter the crystal lattice of strontium fluoride with its simultaneous doping with a rare-earth element [36].

The lattice constants of heat-treated powders of solid solutions can be described by the equation $a = a_0 - kx$, where $a_0 = 5.800 \, Å$ (SrF_2 lattice constant), x — is the dope additive concentration in mole fractions, $k = 0.093$, which is in good agreement with the value $k = 0.089$ for the concentration dependence of the lattice constant of the solid solution $Sr_{1-x}Eu_xF_{2+x}$ [38].

Transmission electron microscopy of the sample $Sr_{0.9}Eu_{0.1}F_{2.1}$ after drying at a temperature of $45°C$ revealed two particle morphologies: spherical particles with a diameter of approximately 18 nm and shapeless flat particles with an average size of approximately 110 nm
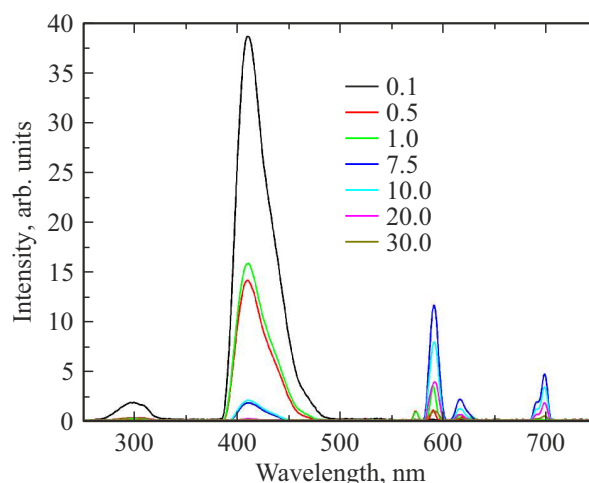
(Fig. 3, *a*). The coherent scattering region corresponds to single particles according to TEM data, which was previously observed in the paper [33]. The TEM image of the sample $Sr_{0.9}Eu_{0.1}F_{2.1}$ after heat treatment at $600°C$ is shown in Fig. 3, *b*. Transmission electron microscopy revealed one morphology of round particles with a diameter of approximately 46 nm, which corresponds to the size of the CSR and was previously noted in the paper [33].

X-ray luminescence spectra were recorded upon excitation by X-ray tubes with silver (Fig. 4) and tungsten (Fig. 5) anodes for synthesized samples of $SrF_2:Eu$ solid solutions.

In the X-ray luminescence spectra upon excitation by a tube with a silver anode, characteristic luminescence bands
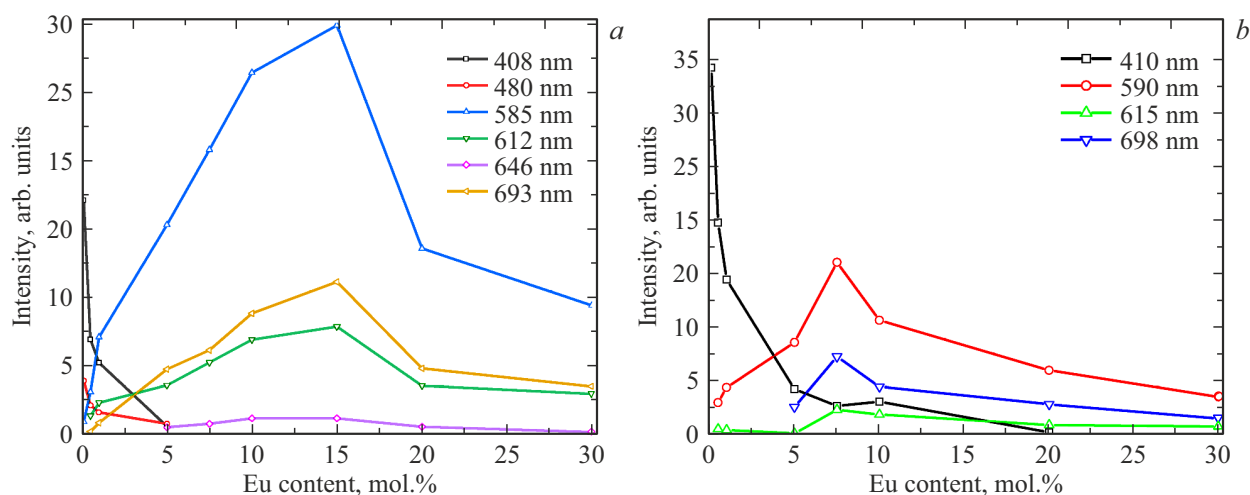
Figure 6. Dependences of the intensity of X-ray luminescence on the content of europium in the solid solution SrF₂:Eu: *a* — upon excitation by an X-ray tube with a silver anode, *b* — upon excitation by an X-ray tube with a tungsten anode. The numerical values of the maxima of the luminescence bands for which the luminescence intensity was determined are presented in the figures.

were revealed that correlate with the intrinsic luminescence band of strontium fluoride (300 nm), attributed to a self-trapped exciton [39] of trivalent europium (585, 612, 646 and 693 nm) [40], as well as divalent europium (411 and 480 nm) [40]. Similar bands were recorded in case of excitation by an X-ray tube with a tungsten anode, but in this case, the intensities of the luminescence bands of the self-trapped exciton and Eu^{2+} are noticeably increased relative to the bands of Eu^{3+}. The most intense luminescence band of trivalent europium is the $^5D_0 \rightarrow ^7F_1$ transition with a maximum at approximately $585-590$ nm. The $^5D_0 \rightarrow ^7F_4$ transition with a maximum at approximately $690-700$ nm has a luminescence intensity that is 2.5 times lower, and the $^5D_0 \rightarrow ^7F_2$ transition with a maximum at approximately $612-615$ nm is 5.5 times less intense than the $^5D_0 \rightarrow ^7F_1$ transition.

The dependences of the intensities of the luminescence bands on the europium content are shown in Fig. 6. With an increase in the content of europium, there is a decrease in the intensity of X-ray luminescence of divalent europium, which agrees with the data [30]. This indicates a decrease in the concentration of Eu^{2+} with an increase in the total concentration of europium, which may be due to a decrease in the concentration of single europium ions, which do not have F^- interstitial ions in the nearest environment that compensate for the excess charge of the trivalent cation. The luminescence intensity of trivalent europium reaches a maximum at a europium content of approximately 15.0 mol.% in case of excitation with an X-ray tube with a silver anode (Fig. 6, *a*) and 7.5 mol.% with excitation with an X-ray tube with a tungsten anode (Fig. 6, *b*). Thus, information has been obtained on the optimal range of europium concentrations for X-ray luminescent particles intended for embedding into diamond in order to form scintillation composites

Conclusion

Single-phase nanopowders of solid solutions SrF₂:Eu with europium content from 0.1 to 30.0 mol.% with particle size ≈ 50 nm were synthesized by precipitation from aqueous solutions. Under X-ray excitation, there were luminescence bands corresponding to the intrinsic luminescence of the strontium fluoride matrix and the luminescence of europium in the di- and trivalent states. The highest X-ray luminescence intensities upon excitation by an X-ray tube with silver and tungsten anodes are demonstrated by compositions with europium content of about 15.0 and 7.5 mol.%, respectively. Meanwhile, the luminescence intensity of powders with optimal concentrations of europium is $2-10$ times higher than the similar intensity of other synthesized powders.

The revealed variability of the luminescence bands and the dependence of their intensities on the europium concentration allow to use the synthesized nanopowders of SrF₂:Eu solid solutions to create polyfunctional diamond composites based on them, promising for electroluminescent films [19,41], visualizers and scintillators of high-intensity X-ray radiation at facilities such as the European X-ray free-electron laser (XFEL) and synchrotrons [9,42].

Conflict of interest

The authors declare that they have no conflict of interest.

References

[1] K. Zhukovsky. Radiation Physics and Chemistry, **189**, 109698 (2021).

[2] H.O. Jönsson, C. Östlin, H.A. Scott, H.N. Chapman, S.J. Aplin, N. Tímneanu, C. Caleman. High Energy Density Physics, **26**, 93−98 (2018).

[3] S.V. Borovykh, A.A. Mityureva, V.V. Smirnov. Phys. Lett. A, **389**, 127088 (2021).

[4] Y. Joo, Y. Park, H. Heo, J. Heo, S-S. Park, S.-H. Kim, K.-H. Kim, H.-S. Kang, H.-S. Lee, S. Noh. Nuclear Instruments and Methods in Physics Research Section A, **843**, 50−60 (2017).

[5] H. Yang, G. Kim, H.-S. Kang. Nuclear Instruments and Methods in Physics Research Section A, **911**, 51−54 (2018).

[6] A. Ghaith, M.-E. Couprie, D. Oumbarek-Espinos, I.A. Andriyash, F. Massimo, J.A. Clarke, M. Courthold, V. Bayliss, A. Bernhard, M. Trunk. Phys. Rep., **937**, 1−73 (2021).

[7] T. Pikuz, A. Faenov, T. Matsuoka, S. Matsuyama, K. Yamauchi, N. Ozaki, B. Albertazzi, Y. Inubushi, M. Yabashi, K. Tono. Scientific Rep., **5**, 17713 (2015).

[8] T. Kurobori, Y. Miyamoto, Y. Maruyama, T. Yamamoto, T. Sasaki. Nuclear Instruments and Methods in Physics Research Section B, **326**, 76−80 (2014).

[9] V. Sedov, S. Kuznetsov, A. Martyanov, V. Ralchenko. Functional Diamond, **2** (1), 53−63 (2022). DOI: 10.1080/26941112.2022.2071112

[10] S.V. Kuznetsov, V.S. Sedov, A.K. Martyanov, S.C. Batygov, D.S. Vakalov, K.N. Boldyrev, I.A. Tiazhelov, A.F. Popovich, D.G. Pasternak, H. Bland, S. Mandal, O. Williams, M.S. Nikova, V.A. Tarala. Ceramics International, **48** (9), 12962−12970 (2022). DOI: 10.1016/j.ceramint.2022.01.169

[11] S.V. Kuznetsov, V.S. Sedov, A.K. Martyanov, S.Ch. Batygov, D.S. Vakalov, S.S. Savin, V.A. Tarala. Ceramics International, **47** (10, Part A), 13922−13926 (2021). DOI: 10.1016/j.ceramint.2021.01.259

[12] V.S. Sedov, S.V. Kuznetsov, V.G. Ralchenko, M.N. Mayakova, V.S. Krivobok, S.S. Savin, K.P. Zhuravlev, A.K. Martyanov, I.D. Romanishkin, A.A. Khomich. Diamond and Related Materials, **72**, 47−52 (2017).

[13] A. Snigirev, V. Kohn, I. Snigireva, B. Lengeler. Nature, **384** (6604), 49−51 (1996).

[14] T.V. Kononenko, V.G. Ralchenko, E.E. Ashkinazi, M. Polikarpov, P. Ershov, S. Kuznetsov, V. Yunkin, I. Snigireva, V.I. Konov. Appl. Phys. A, **122** (3), 152 (2016).

[15] Y. Shvyd´ko, V. Blank, S. Terentyev. MRS Bulletin, **42** (6), 437−444 (2017).

[16] R.S. Balmer, J.R. Brandon, S.L. Clewes, H.K. Dhillon, J.M. Dodson, I. Friel, P.N. Inglis, T.D. Madgwick, M.L. Markham, T.P. Mollart. J. Physics: Condensed Matter., **21** (36), 364221 (2009).

[17] I. Aharonovich, E. Neu. Advanced Opt. Mater., **2** (10), 911−928 (2014).

[18] T.A. Railkar, W.P. Kang, H. Windischmann, A.P. Malshe, H.A. Naseem, J.L. Davidson, W.D. Brown. Critical reviews in solid state and materials sciences, **25** (3), 163−277 (2000).

[19] J.-X. Chen, X.-P. Wang, L.-J. Wang, X.-W. Yang, Y. Yang. J. Luminescence, **224**, 117310 (2020).

[20] A. Magyar, W. Hu, T. Shanley, M.E. Flatt´e, E. Hu, I. Aharonovich. Nature Commun., **5** (1), 1−6 (2014).

[21] D.E. Vanpoucke, S.S. Nicley, J. Raymakers, W. Maes, K. Haenen. Diamond and Related Materials, **94**, 233−241 (2019).

[22] V.S. Sedov, A.K. Martyanov, A.A. Khomich, S.S. Savin, E.V. Zavedeev, V.G. Ralchenko. Diamond and Related Materials, **109**, 108072 (2020). DOI: 10.1016/j.diamond.2020.108072

[23] V. Sedov, S. Kouznetsov, A. Martyanov, V. Proydakova, V. Ralchenko, A. Khomich, V. Voronov, S. Batygov, I. Kamenskikh, D. Spassky, S. Savin, P. Fedorov. ACS Appl. Nano Mater., **3** (2), 1324−1331 (2020).

[24] B.P. Sobolev. *The Rare Earth Trifluorides: The High Temperature Chemistry of the Rare Earth Trifluorides* (Institut D´Estudis Catalans, 2000).

[25] B.P. Sobolev, K.B. Seiranian. J. Solid State Chem., **39** (3), 337−344 (1981).

[26] B.P. Sobolev, P.P. Fedorov. J. Less Common Metals, **60** (1), 33−46 (1978).

[27] B.P. Sobolev, N.L. Tkachenko. J. Less Common Metals, **85**, 155−170 (1982).

[28] L.A. Olkhovaya, P.P. Fedorov, D.D. Ikrami, B.P. Sobolev. J. Thermal Analysis, **15** (2), 355−360 (1979).

[29] I.I. Buchinskaya, P.P. Fedorov. Russian Chemical Rev., **73** (4), 371−400 (2004).

[30] J. Peng, S. Hou, X. Liu, J. Feng, X. Yu, Y. Xing, Z. Su. Materials Research Bulletin, **47** (2), 328−332 (2012).

[31] T. Krahl, F. Beer, A. Relling, K. Gawlitza, K. Rurack, E. Kemnitz. ChemNanoMat, **6** (7), 1086−1095 (2020).

[32] M. Heise, G. Scholz, T. Krahl, E. Kemnitz. Solid State Sci., **91**, 113−118 (2019).

[33] Y.A. Ermakova, D.V. Pominova, V.V. Voronov, A.D. Yapryntsev, V.K. Ivanov, N.Y. Tabachkova, P.P. Fedorov, S.V. Kuznetsov. Dalton Transactions, **51** (14), 5448−5456 (2022).

[34] S. Kuznetsov, Y. Ermakova, V. Voronov, P. Fedorov, D. Busko, I.A. Howard, B.S. Richards, A. Turshatov. J. Materials Chem. C, **6** (3), 598−604 (2018).

[35] Z. Zhou, W. Li, J. Song, G. Yi, B. Mei, L. Su. Ceramics International, **44** (4), 4344−4350 (2018).

[36] Y.A. Rozhnova, S.V. Kuznetsov, A.A. Luginina, V.V. Voronov, A.V. Ryabova, D.V. Pominova, R.P. Ermakov, V.A. Usachev, N.E. Kononenko, A.E. Baranchikov, V.K. Ivanov, P.P. Fedorov. Materials Chem. and Phys., **172**, 150−157 (2016).

[37] R.D. Shannon. Acta crystallographica section A, **32** (5), 751−767 (1976).

[38] P.P. Fedorov, B.P. Sobolev. Crystallogr. Rep., **37** (5), 1210 (1992). (in Russian).

[39] T. Demkiv, M. Chylii, V. Vistovskyy, A. Zhyshkovych, N. Gloskovska, P. Rodnyi, A. Vasil´ev, A. Gektin, A. Voloshinovskii. J. Luminescence, **190**, 10−15 (2017).

[40] M.Y.A. Yagoub, H.C. Swart, E. Coetsee. Vacuum, **191**, 110362 (2021).

[41] H.-J. Chen, X.-P. Wang, L.-J. Wang, X.-L. Ke, R.-M. Ning, M.-L. Song, L.-H. Liu. Carbon, **109**, 192−195 (2016).

[42] V. Sedov, S. Kuznetsov, I. Kamenskikh, A. Martyanov, D. Vakalov, S. Savin, E. Rubtsova, V. Tarala, S. Omelkov, A. Kotlov, V. Ralchenko, V. Konov. Carbon, **174**, 52−58 (2021). DOI: 10.1016/j.carbon.2020.12.020

Translated by E.Potapova